SHEAR STRENGTH OF THE ASDEX UPGRADE TF COIL INSULATION: RUPTURE, FATIGUE AND CREEP BEHAVIOUR

B. Streibl, E.A. Maier, J. Perchermeier

IPP 1/230

March 1987

MAX-PLANCK-INSTITUT FÜR PLASMAPHYSIK

8046 GARCHING BEI MÜNCHEN

MAX-PLANCK-INSTITUT FÜR PLASMAPHYSIK
GARCHING BEI MÜNCHEN

SHEAR STRENGTH OF THE ASDEX UPGRADE TF COIL INSULATION: RUPTURE, FATIGUE AND CREEP BEHAVIOUR

B. Streibl, E.A. Maier, J. Perchermeier

IPP 1/230 March 1987

Die nachstehende Arbeit wurde im Rahmen des Vertrages zwischen dem Max-Planck-Institut für Plasmaphysik und der Europäischen Atomgemeinschaft über die Zusammenarbeit auf dem Gebiete der Plasmaphysik durchgeführt.

SHEAR STRENGTH OF THE ASDEX UPGRADE TF COIL INSULATION: RUPTURE, FATIGUE AND CREEP BEHAVIOUR

B. Streibl, E.A. Maier, J. Perchermeier
Max-Planck-Institut für Plasmaphysik, EURATOM Association
D-8046 Garching, Fed. Rep. Germany.

P.L. Cimbrico, G. Varni, D. Pisani
ANSALDO Componenti, Genova, Italy

R. Deska, J. Endreat
MAN-NT, Munich, Fed.Rep. Germany

R. Schäfer
IABG, Ottobrunn, Fed.Rep. Germany

Abstract

This report is concerned with the interlaminar shear strength of the insulation system for the 16 toroidal field (TF) coils of ASDEX Upgrade. The interlaminar shear properties of the glass-epoxy insulation are primarily determined by the resin system (ARALDIT-F, HT 907, DZ 40) and its curing procedure. The pure resin was therefore tested first in tension. The results were taken into account for setting up the method of curing the TF coils. Shear tests of the complete glass-epoxy system were then conducted with tubular torque specimens providing a nearly homogeneous stress distribution. In particular, the influence of the amount of flexibilizer (5, 10, 15 parts of resin weight = PoW) on the rupture and fatigue strengths was assessed at a temperature T = 60 C, as also was the temperature dependence of the creep rate (40 C, 60 C, 80 C). The results obtained are not based on safe statistics. Nevertheless, they show clear trends.

Finally, a visco-elastic (dashpot spring) model was set up to describe the creep behaviour of the insulation system.

1. INTRODUCTION

Supporting the TF coil forces near the toroidal centre without any external structure considerably increases the potential of a tokamak. As a consequence of such a design, as chosen for ASDEX Upgrade, the individual turns of a TF coil [4] have to be bonded via the glass-epoxy insulation to achieve the required mechanical rigidity. This bond, in turn, is exposed to sizeable mechanical stresses - up to 20 Mpa of interlaminar shear to transfer the forces between adjacent turns and up to 70 Mpa of vault compression to equilibrate the centering forces of each TF coil. The peak of the shear stress, resulting from a torque, limits the experimental parameter range [4]. This calls for a testing method permitting clear interpretation and insight into the governing material behaviour. For the given stress distribution one can focus on shear since the compressional stresses are modest and rather contribute to increasing the shear strength [2]. The usual lap shear specimens loaded either by tension or compression forces exhibit an inhomogenous stress distribution [2]. It is not feasible either to measure the shear angle (γ) quantitatively. However, the quantitative knowledge of γ is required in order to assess the

- mechanical properties like shear modulus (G) and rupture ductility;

- rupture behaviour during cycling, i.e. the hysteresis and the change of G;

- creep characteristics, i.e. the long-term displacement behaviour.

The mechanical tests were thus based on thin-walled tube specimens [2] loaded by an axial torque. The tests were executed at MAN-NT, where one of the rare test devices exclusively developed for insulation tube specimens is available [1].

The agent transferring shear between the layers of glass fabric (interlaminar shear) and the copper surface (chemical adhesion) is the epoxy resin. The resin thus dominates the mechanical behaviour since it is the weakest link in this chain. Epoxy resin is of poor ductility. Internal strains and the homogeneity of polymerization therefore considerably affect its fatique strength. An elaborate curing method and a careful choice of the flexibilizer (flex) content are therefore mandatory. However, the addition of flex reduces the glass transition point (T_G) of the resin system linearly from T_G = 135 C, without any flex, down to T_G = 95 C, with 15 PoW flex. Though the nominal operating temperature of the TF coils is as low as 40 C, the potential for a larger temperature range has to be maintained. The impact of the flex content on the mechanical properties was therefore assessed up to 80 C.

Epoxy resins strongly deviate from Hooke's law. Owing to the small difference between T_G and the working temperature there is pronounced creep behaviour. Unfortunately, it is not feasible by cyclic testing to simulate the genuine loadshape for the envisaged number of cycles (N = 20,000). For the TF magnet the average pulse length under full shear load will be $t_L \approx 5$ s, followed by an interval of $t_R \gtrsim 600$ s, during which a major part of the creep will relax. The shear fatique tests, however, were run with a sinusoidal load shape of period P = 4 s ($t_L = t_R = 2$ s). To be able to relate the results of these tests to the actual load shape, allowing also for creep, a quantitative description of the material behaviour is required.

2. TENSION TESTS WITH PURE RESIN SPECIMENS

2.1 Resin System

The resin system contains only standard CIBA products. To provide at least 12 h of low viscosity for coil impregnation, the resin mixture does not contain any accelerator. The basic constituents are the epoxy resin ARALDIT-F (100 PoW) and the hardener HT 907 (80 PoW). The resin system is gelified (forming of macromolecules) at 100 C and cured (cross linking) at 145 C for 36 h. The gelification time has to allow for the flex (F) content. With 5 PoW of flex (F5) a time of 36 h is required; for F 10 and F 15 an increase to 44 h and 46 h, respectively, is required.

2.2 Preparation of Resin Specimens

RESIN SPECIMENS

ANSALDO Genova, the manufacturer of the TF coils, provided all insulation specimens. The ASTM D 638 resin specimens were machined from conical rods cast in an aluminium mould. The resin rods were cooled down in air after curing. The finished specimens showed internal stresses in polarized light. It is unlikely that these stresses are caused by machining in view of the resulting stress pattern. The stresses could be relieved by heat treatment (tempering): holding the specimens at 145 C for 6 h and then slow oven-cool down over 12 h.

2.3 Results of Fatigue Tests (Fig. 1)

The fatigue tests were conducted by IABG Ottobrunn with zero to maximum load cycles (f = 0.15 Hz) at a temperature of 40 C. Only 2 to 3 specimens were available for each parameter tested.

The target of the first series (non-tempered) was to test the influence of the flex content on the fatigue life (N_B). As can be seen on the left-hand side of Fig. 1, increasing the amount of flex results in a reduction of the scatter band width. The average number of rupture cycles (N_{BA}) are smallest for the F0 specimen. The second series was thus limited to comparison of the F 5 and F 10 specimens (non-tempered) at a higher N_B. The middle of Fig. 1 shows for this case an increase of the scatter band and the superiority of the F 10 specimen.

The target of the last series (right-hand side of Fig. 1) was to investigate with the F 5 specimen the impact of tempering and curing on the scatter band. By adding an accelerator (0.1 PoW = A 0.1 and 0.5 PoW = A 0.5) with unchanged curing parameters, the polymerization rate was increased and the curing temperature reduced. Owing to the internal stress relief there is a significant reduction of the scatter band for the tempered specimen. The tempering also entails a modest drop of N_{BA}. This drop is most likely caused by the second heating to 145 C. At this temperature not only are stresses relived owing to the regained movability of the molecule chains above T_G, but also more chains are obviously broken than can be recombined (overcure). The same assumption applies to the drop of N_{BA} due to the addition of accelerator (A 0.5). In this case curing is already completed at 100 C. The heating to 145 C just ages the resin.

3. CURING OF THE TF COILS

From the results of the resin tests the following guidelines are derived for coil curing and operation:

- Overcuring should be avoided.
- The cured coil ought not to be heated beyond T_G.
- Internal strains have to be homogenized (relieved) by a low cool-down rate; technical effort is required to keep them at the lowest possible initial level.

The density-temperature diagram [3] of Fig. 2 for liquid, gel and solid resin immediately shows that only a small fraction of linear shrinkage can be prevented from transforming into an internal strain since the shrinkage of resin is about 10 times as large as the corresponding thermal expansion of the copper turns. Hence at least 1.2% of cool-down shrinkage transforms into strain. It is only possible to avoid strains by the 0.6% of shrinkage from the liquid to the gel condition which would originate in combination with unfavourable temperature gradients. Usually coils are impregnated with resin at a

lower temperature than that of gelification and are afterwards heated by the heaters of the autoclave to the gelification temperature. The heat transport to the coil turns thus requires a temperature gradient via the coil insulation (Fig. 3), and gelification will be started on the hotter coil outside, where the resin pool is. This, in turn, blocks the inflow of resin, required for compensating the liquid-gel density rise, and strain concentrations must originate inside the coil. To avoid this, the TF coils will be heated to the gelification temperature (100 C) prior to resin impregnation, which is possible owing to the absence of accelerator. Additionally, the coil turns will be heated electrically during gelification to enforce the onset of gelification inside the coils. A few centigrades of temperature rise are sufficient to achieve this target since $\Delta T = 10$ C already doubles the polymerization rate.

4. HARDWARE OF TORSIONAL TESTS

4.1 Test Device

The axial torque is produced by a hydraulic piston on the top of the device and is transmitted to the specimen via cardanic hinges (Fig. 4). An additional piston on the bottom is able to exert axial tension or compression force. The specimens are heated to the testing temperature by air. A mantle surrounding the specimens is tightened against the cylindrical clamping elements to guide the air circulation and to reduce heat losses. The test device was exclusivley applied in a moment-controlled mode.

4.2 Specimen

There were two kinds of specimens developed:

- long tube specimens for parametric studies. These specimens can be fabricated on a laboratory scale;
- short tube specimens which could also be cut out of a destroyed coil.

A long tube specimen consists, in principle, of a copper tube 300 mm in length, cut at half-length normal to its axis and rebonded via an annulus of insulation with an axial width of 1.6 mm. The annulus is composed of many layers of glass fabric which are then vacuum-impregnated with resin (50% of total volume). The device for aligning and impregnating (in the vertical position) the long tube specimen is shown in Fig. 5. The copper tubes are precisely lathed on the bonding surface to an outer diameter of 69

mm and a wall thickness of 6 mm. The surplus resin of the cured specimen is removed by machining and the surface of the insulation annulus sealed by a cold-curing resin.

The second type of specimens are machined from paired copper plates bonded via insulation. The plate thickness of 32 mm corresponding to the conductor thickness of a TF coil provides tubes 64 mm in length. These specimen plates will be inserted into the casting mould during TF-coil fabrication to provide specimens for quality control purposes. The short tube specimens are inserted into a holder and bonded to it with an overlap of 25 mm (Fig. 6). The tests performed up to now have not shown any systematic difference between short and long tube specimens.

4.3 Stress and Strain Pick-up

The tube dimensions prescribe a linear strain variation of less than $\pm 10\%$. However, the stress distribution will homogenize under strain owing to creep. All stress values quoted are therefore average quantities which were derived from the signal of the moment transducer by the relation

$$< \sigma >= \frac{12 M_t}{\pi (d_o^3 - d_I^3)}$$

M_t : torque
d_o, d_I : outer and inner specimen diameter
$< \sigma >$: average shear stress.

The strain is measured with a temperature-compensated inductive displacement transducer via the relative displacement of two rings fixed to the copper sections at a distance of 1.5 mm from the insulation gap boundaries (Fig. 4). The contribution of the copper shear angle to the transducer signal is less than 15%. This contribution is linearly dependent on the torque and can thus be properly eliminated.

5. RESULTS OF RUPTURE TESTS WITH INSULATION TUBE SPECIMENS

All tests were executed at the same shear velocity of about 1 Mpa/s (linear). A typical plot of the shear stress (σ) versus shear angle (γ) of a ruptured F 10 specimen is shown in Fig. 7. None of the specimens ruptured adhesivley. In most cases rupture occurred near the copper surface, but throughout with a layer of resin remaining on the metal. Obviously, the rupture starts at the transition zone between the flexible lamella

structure, formed normal to the metal surface, and the less flexible globular bulk of the resin [5]. Specimens ruptured after a preceding creep test (20 Mpa for 100,000 s) did not show noticeable deterioration compared with virgin specimens. The test results obtained are listed in Table I. They can be interpreted as follows:

- The higher the temperature, the smaller the rupture shear.
- More than 5 PoW flex yields 20% better results. Within the scatter of results F 10 and F 15 specimens do not differ in strength.
- The shear angle at the stress maximum is around 3%, i.e. 6% for the resin.

Flex content [PoW]	Test temperature [C]	Rupture stress [Mpa]	Rupture strain [%]
F 5	40	49	3.6
	60	36.5	3.5
F 10	60	47	3.4
F 15	60	43	3.3

Table I: Results of rupture tests with tube specimens (mean values)

6. RESULTS OF FATIGUE TESTS WITH INSULATION TUBE SPECIMENS

The fatigue tests were performed throughout at T = 60 C with zero to maximum load of frequency f = 1/4 Hz. Prior to cycling each specimen was subjected to a creep test of 10,000 s duration at $\sigma = 20$ Mpa. During cycling the load was increased every N = 20,000 cycles by an increment of 5 Mpa, starting from $\sigma = 20$ Mpa.

The shearing displacements (γ) at the upper (γ_U) and lower (γ_L) load levels are plotted in Fig. 8. The remaining shear displacement at zero load, caused by creeping, quickly grows during the first few cycles. After a few hundred cycles the growth rate becomes constant and consequently the creep displacement rises linearly furtheron. The displacement amplitude ($\gamma_U - \gamma_L$) remains stable until the rupture load level is reached. The rupture load level shows the following properties:

- The creep rate is significantly larger than would be predicted by extrapolation from the preceding load levels. The hysteresis plot of Fig. 9 shows for the F 15

specimen, step 3, a non-zero hysteresis width, i.e. a detectable creep displacement per cycle. The hysteresis width grows with the number of cycles until a constant creep rate is established.

- Rupture is preceded by a restarting growth of the creep rate and consequently the hysterisis area. Additionally, the shear modulus (G_{EL}), the inclination of the hysteresis curve, significantly drops (F 5 specimen of Fig. 9) and thus entails a rising γ-amplitude (Fig. 8 lower left-hand part).

These observations suggest the following rupture mechanism. During the initial cycles creep is not able to homogenize the internal stress distribution since the creep time constant (τ) is much larger than the priod of a load cycle. Consequently, a certain number of overstressed chains rupture.

Now two differenc scenarios can be imagined:

- For each ruptured molecule chain a larger number of not yet stressed chains take over the load and finally the molecule rupture will stop (stable stress level). The more regular the polymerisation pattern is the less chains will rupture during the rise of the load. The higher the stress level, the more chains will rupture before equilibrium is achieved.

- At too high a stress level rupture can no longer be stopped. After a certain number of cycles a constant rupture rate is established until the resource of little stressed molecule chains is exhausted. Then the rupture rate starts to grow causing the complete failure of the specimen (unstable stress level).

However, also at the so-called stable stress level creep will finally cause failure. (An infinitely large creep displacement can only be imagined for a liquid.) In fact, in [5] a critical creep displacement (γ_c) after which rupture occurs is postulated and measured for a non-laminated epoxy resin system. Presumably near γ_c the creep ability of a growing number of molecules becomes exhausted. The interaction forces with their surrounding decay and the load of the remaining, still creeping molecules is increased. Since during the preceding creeping period an optimum load distribution had been established, this process instably grows and causes rupture. This creep instability must then also occur at lower load levels provided that the loading period is sufficiently long to arrive at γ_c. An additional consequence of a critical shear displacement is that also the ratio of load to relaxation time (t_L/t_R) must influence the fatigue life since part of the creep is reversible.

For the F 5 specimen the test results show a comparatively poor fatigue strength. None of the three specimens tested had survived more than 3000 cycles at step 1. Between the F 10 and F 15 specimens there was no detectable difference in fatigue strength. All specimens survived $N > 19,000$ cycles at step 2 (25 Mpa). The best result, shown in Fig. 8, was obtained for a F 15 specimen. The addition of flex obviously leads to a more regular cross-linking distribution which homogeneously spreads the load to a larger number of molecule chains. The overall cross-linking density, represented by T_G, does not seem to influence the fatigue strength as long as the molecule chains remain rigid ($T < T_G$). Above a critical cross-linking density irregularities and most likely crystallites [6] deteriorating the mechanical strength, seem to be formed during polymerization.

In spite of the small number of F 10/F 15 specimens tested an N = 20,000 fatigue strength of 25 Mpa is derived for the chosen insulation system up to T = 60 C. (Note that step 1 cycling is roughly equivalent to 12,000 cycles at step 2.) Better statistics will be established during fabrication by testing the specimens cured together with each TF coil.

7. RESULTS OF CREEP TESTS WITH INSULATION TUBE SPECIMENS

The TF coils will mainly be loaded in a single direction. The contribution of creep to the elastic displacement has therefore to be known.

The creep tests included a $\sigma = 20$ Mpa load period of 100,000 s followed by a relaxation period (at zero load) of up to 50,000 s. The typical shape of the shear angle resulting from such a creep test is demonstrated in Fig. 10. During the sudden rise of the load the elastic shear modulus (G_{EL}) can be determined from the immediate response of the shear angle. The same holds for the unloading after t_L=100,000 s. The modulus is independent of temperature $G_o \sim$ 3500Mpa. The creep strain can be separated from the total strain as indicated by the dashed line in Fig. 10. For F 5 specimens the creep strain is plotted in Fig. 11 for temperatures of 40 C, 60 C, and 80 C. Even for T = 80 C the measured maximum creep strain would not affect the operation of the TF magnet. At T = 60 C the elastic strain (γ_{EL}) approximately coincides with the creep displacement, hence the total strain is two times the elastic strain.

At 60 C a F 10 specimen was also tested, which showed the same basic shape of the strain versus time plot as the F 5 specimen, but at a 20% reduced creep level. During loading

obviously a smaller number of molecule chains were ruptured due to the increased amount of flex. Hence, consistently with the rupture and fatigue results the creep test also shows an advantage of 10 to 15 PoW flex compared with 5 PoW.

8. VISCOUS (DASHPOT) MODEL

The creep tests provide valuable information for quantitatively assessing the material behaviour of epoxy resin. The following considerations are based on a linear creep model. However, a correction is suggested allowing for non-linear creep.

8.1 Essentials of the Model

Creep is a time and temperature-dependent phenomenon. The description of the temperature dependence is based on the theory of thermal oscillators moving in a lattice with voids after surmounting a potential barrier [6]. A minimum of two different potential barriers is required for defining a time constant. For each further time constant an additional potential barrier has to be assumed [8]. The interaction between the potential barriers can be expressed by spring dashpot models with temperature-dependent elements. Numerous spring-dashpot models are presented in [6, 7], which are equivalent, though their spring dashpot combination looks different. The model of Fig. 12 was chosen because its arrangement directly reflects the basic properties of the test results. The essentials of this model are:

- The steady-state condition at constant load is a constant creep rate. This behaviour is typical of all plastics.

- Elastic and creep elements are strictly separated because their temperature dependence is different.

- The fit to the test results requires a minimum of two time constants. There is a comparatively short one (τ_1), which is hard to identify in Fig. 11. Depending on the temperature, it amounts to $(\tau_1)_{T=40C} \approx 280$ s, $(\tau_1)_{80} \approx 100$s. A contrary dependence on temperature results for the second, much longer time constant $(\tau_2)_{40} \approx 1.3h; (\tau_2)_{80} \approx 3.1h$.

8.2 Shortcomings of the Model

A model with linear elements (no dependence on stress or strain) can only describe the irreversible part (γ_I) of the creep by

$$\gamma_I = \dot{\gamma}_\infty \cdot t \ldots \tag{1}$$

$\dot{\gamma}_\infty$: steady-state creep rate t: time.

The γ_I of Fig. 11 is a factor of 1.5 to 2.2 as large as the linear value. This nonlinearity misleads one into assuming different time constants for the reversible creep (γ_R) during the load and relaxation period of Fig.11.

For fitting the temperature dependence of the test results the relations of [6] were partially extended in a somewhat arbitrary way by adding probability terms of the form $e^{-T_0/T}$, where T_0 is a constant temperature representing a potential barrier $\Delta U = kT_0$.

According to [9] there is great uncertainty with respect to the temperature dependence of the bounce frequency (ν). There are arguments both for an increase and decrease of ν with temperature. The contrast in temperature dependence between τ_1 and τ_2 shown by the test results strongly indicates that both possibilities exist within a macro molecule structure and that the assumption of [6]

$$\nu \propto T$$

has to be modified. In order to allow also for decaying characteristics T is additionally devided by a probability term.

For the fast circuit (γ_1) the following relations are introduced:

For the spring representing the shear modulus:

$$G_1 = G_{01} T e^{T_{G1}/T} \ldots \tag{2}$$

where G_{01} and T_{G1} are constants which have to be determined from the test results.

For the time constant of the fast circuit

$$\tau_1 = \frac{\tau_{01}}{T} e^{T_{01}/T} \ldots \tag{3}$$

The index 0 again designates a constant.

The viscosity (η) of the damper then becomes

$$\eta_1 = \tau_1 G_1 \ldots \tag{4}$$

For the slow circuit (γ_2) the viscosities are described by

$$\eta_2 = \eta_{20} e^{T_{20}/T}; \eta_3 = \eta_{30} e^{T_{30}/T} \ldots \tag{5}$$

and the spring becomes similar to eq.(2)

$$G_3 = G_{03} T e^{T_{G3}/T} \ldots \tag{6}$$

For defining the constants of the relations (2) to (6) two temperature plots of Fig. 11 are required. The third one can be taken for checking the accuracy of the relations.

8.3 Differential Equations

For the quick circuit it follows from Fig. 12 that

$$\dot{\gamma}_1 = \frac{1}{\tau_1}\left(\frac{\sigma}{G_1} - \gamma_1\right) \ldots \tag{7}$$

The dot denotes a time derivative. For the slow circuit one obtains

$$\ddot{\gamma}_2 + \dot{\gamma}_2/\tau_2 = \frac{\sigma G_3}{\eta_2 \eta_3} + \frac{\dot{\sigma}}{\eta_2} \ldots \tag{8a}$$

with

$$\tau_2 = \frac{\eta_3/G_3}{1+\alpha}; \alpha = \frac{\eta_3}{\eta_2} \ldots \tag{8b}$$

With $\tau_2 \gg \tau_1$ the total creep displacement $\gamma = \gamma_1 + \gamma_2$ is then given by

$$\dddot{\gamma} \cdot \tau_1 \cdot \tau_2 + \ddot{\gamma} \cdot \tau_2 + \dot{\gamma} = \frac{\sigma}{\eta_2 + \eta_3} + \dot{\sigma}\left(\frac{\tau_2}{\eta_2} + \frac{1}{G_1}\right) + \ddot{\sigma}\frac{\tau_2}{G_1} \ldots \tag{9}$$

The elastic displacements

$$\gamma_{EL} = \frac{\sigma}{G_{EL}} \ldots \tag{10}$$

finally have to be added to a solution of (9).

8.4 Determination of the Model Elements (Fig. 12) by Means of the Creep Test (Fig. 11)

With $\dot{\sigma} = 0$ and $\tau_2 \gg \tau_1$ the solution of (9) for the creep test becomes

- for the loading period

$$\gamma_L = \gamma_{R1}\left(1 - e^{-t/\tau_1}\right) + \gamma_{R2}\left(1 - e^{-t/\tau_2}\right) + \dot{\gamma}_\infty t_1 \ldots \tag{11a}$$

- for the decay during relaxation

$$\gamma_D = \gamma_I(t_{LE}) + \gamma_{R1} e^{-t_R/\tau_1} + \gamma_{R2} e^{-t_R/\tau_2} \ldots \tag{11b}$$

with the abbreviations

$$\dot{\gamma}_\infty = \frac{\sigma}{\eta_2 + \eta_3}; \quad \gamma_{R1} = \frac{\sigma}{G_1}; \quad \gamma_{R2} = \frac{\sigma/G_3}{1+\alpha}; \dots \tag{11c}$$

for $t_L \gg \tau_2$ the total reversible strain becomes

$$\gamma_{R\infty} = \gamma_{R1} + \gamma_{R2} \dots \tag{11d}$$

At the beginning ($t_L = 0$) of the load period $\gamma_L = 0$ was set. At its end ($t_L = t_{LE}, \gamma_L = \gamma_{LE}$) steady-state conditions are achieved ($t_{LE} \gg \tau_2$) and $\dot{\gamma}_\infty$ can be determined from Fig. 11. The relaxation period, starting at $t_R = 0$, i.e. $t_L = t_{LE}$, was also run for $t_R \gg \tau_2$. The sum of the irreversible (γ_I) and reversible ($\gamma_{R\infty}$) creep strains thus yields γ_{LE}. This condition was assumed for eq.(11b).

With eq. (11c, d), the elements of the creep model are not yet completely determined. Additionally, the quantities τ_2 and γ_{R2} have to be drived from the strain plots for $\tau_1 \ll t_R < \tau_2$, where $\gamma_1 \approx 0$ holds, together with the quantity τ_1 at $t_R < \tau_1$, where $\gamma_2 \approx 0$ holds. It then follows that

$$\alpha = \frac{\eta_3}{\eta_2} = \frac{\gamma_{R2}}{\dot{\gamma}_\infty \tau_2}; G_3 = \frac{\sigma/\gamma_{R2}}{(1+1/\alpha)^2} \dots \tag{12a}$$

$$\eta_2 = \frac{\sigma/\dot{\gamma}_\infty}{1+\alpha}; \quad \eta_3 = \frac{\sigma/\dot{\gamma}_\infty}{1+1/\alpha} \dots \tag{12b}$$

In eq. (12) α is a small quantity of size 0.1 to 0.3. The quantities of eq. (11c, d) and eq. (12) were determined at T = 40 C and T = 80 C to find the constants eq. (2) to eq. (6) of the creep model. The results are

$$G_{01} \approx 3 \cdot [Mpa/K]; T_{G1} \approx 3410[K]$$

$$\tau_{01} \approx 14[s \cdot K]; T_{01} \approx 2750[K]$$

$$\eta_{02} \approx 16400[Mpa \cdot s]; T_{02} \approx 2880[K]$$

$$\eta_{03} \approx 15[Mpa \cdot s]; T_{03} \approx 5800[K]$$

$$G_{03} \approx 4.7 \times 10^{-7}[Mpa/K]; T_{G3} \approx 6000[K]$$

The shear moduli are always larger than G_{EL} since $\gamma_{R1}, \gamma_{R2} < \gamma_{EL}$.

8.5 Cyclic Tests, Influence of Frequency on the Strain Amplitude

The period length (P) of a zero to maximum load cycle

$$\sigma = \sigma_A(1 - cos wt); w = 2\pi/P \ldots \tag{13}$$

will always be $P \ll \tau_2$. Hence only the creep amplitude resulting from eq. (7),

$$\gamma_{1A} = \frac{\sigma_A}{G_1} \frac{sin(wt + \varphi)}{\sqrt{1 + (w\tau_1)^2}}; \varphi = \frac{1}{w\tau_1} \ldots \tag{14}$$

can contribute to the hysteresis width. Owing to the $\pi/2$ phase shift ($\varphi \approx 0$) of γ_{1A} the ratio of the hysteresis width for the total displacement is, with good accuracy,

$$\frac{|\gamma_{1A}|}{\gamma_{EL}} = \frac{G_{EL}/G_1}{\sqrt{1 + (w\tau_1)^2}} \approx \frac{G_{EL}/G_1}{w\tau_1} \ldots \tag{15}$$

For P = 4 s and the derived material properties it follows that $\gamma_{1A}/\gamma_{EL} < 0.1\%$. This result means for the plots of Fig. 9 that as soon as a hysteresis can be detected the destruction of the material starts, i.e. specimen failure will occur within less than a few thousand cycles.

The small hysteresis creep is integrated by the damper η_1 until a saturation value γ_{RS1} is reached, whose size depends on the ratio t_L/t_R. The same holds for the second circuit which is "pumped" to γ_{RS2}. The saturation creep is of a reversible nature. It will be discussed for cycles of equivalent rectangular pulse shape.

8.6 Saturation Value of Reversible Creep (γ_{RS})

The saturation value is obtained when the creep displacement originating during t_L just decays during t_R. This equilibrium condition given by eq. (11) yields a similar expression for γ_{R1} and γ_{R2}. For i = 1,2 it follows that

$$\gamma_{RSi} = \gamma_{Ri} e^{-t_R/\tau_i} \left(1 - e^{-t_L/\tau_i}\right) / \left(1 - e^{-t_R(1+t_L/t_R)/\tau_i}\right) \ldots \tag{16a}$$

$$\gamma_{RS} = \gamma_{RS1} + \gamma_{RS2} \ldots \tag{16b}$$

For the fatigue tests, index F, it follows from eq. (16) with $t_L = t_R \ll \tau_1, \tau_2$ that

$$\gamma_{RSF} = \frac{1}{2}\gamma_{R\infty} \ldots \tag{17}$$

This is equivalent to the saturation value of γ_R originating from a constant load of half the upper load level.

For the actual load cycle to which the TF coils will be subjected during operation, index 0, it holds that

$$t_L/t_R < 1/60; \quad \text{and} \quad t_L \ll \tau_1, \tau_2$$

From eq. (16) it follows then that

$$\gamma_{RSO} < \gamma_{R\infty}/200 \approx 0.$$

8.7 Non-linear Part of the Irreversible Creep

In [6] a constant potential energy distribution, defined by potential barriers, was assumed for describing the material behaviour. This assumption leads to a linear creep formulation. However, the test results have shown a considerable contribution of nonlinear, irreversible creep (γ_{IN}) at the stress level of 20 Mpa. Consequently, the potential distribution must have been perturbed during the loading period.

The potential distribution was separated in [6] into potential barriers for reversible (γ_R) and linear, irreversible (γ_I) creep. It is not possible to imagine a change of the irreversible potential distribution since this is not compatible with the constant steady-state creep rate shown by the test results.

However, no contradiction will arise according to [9] with the reversible potential. A remaining perturbation of it would entail after unloading and relaxation a different population of the potential pots. Since the particle difference between the initial and the perturbed population is directly proportional to a creep strain, a perturbation of the reversible potential can explain the nonlinear creep.

The only accessible quantity which can be related to the reversible potential barriers is γ_R. The dashpot model of Fig. 12 represents this quantity by the elongation of the springs. With respect to nonlinear creep this model can be simplified by eliminating the fast circuit (τ_1). Demanding that the reversible steady-state creep ($\gamma_{R\infty}$) remains unchanged, the following expressions transform the relations for the two circuit-model to the one-circuit model.

$$G_3 \rightarrow G_{3N} \quad \text{with}$$

$$1/G_{3N} = 1/G_3 + (1+\alpha)/G_1 \ldots \tag{18a}$$

$$\gamma_{R1} \rightarrow 0; \quad \gamma_{R2} \rightarrow \gamma_{R\infty} \ldots \tag{18b}$$

The simplified one-circuit model describes both the stress acting on the reversible potential barriers and the resulting time-dependent strain (γ_R) by the elongation of the spring G_{3N}.

The nonlinear strain γ_{IN}, originating during the first loading period of the material will therefore be expressed by a polynomial in γ_R. For this virgin material the following conditions further define the polynomial expression

- the initial conditions, postulating the existence of linear behaviour near $\gamma_R = 0$.

Hence,

$\cdot\ \gamma_{IN} = 0$ for $\gamma_R = 0$;

$\cdot\ \partial\gamma_{IN}/\partial\gamma_R = 0$ for $\gamma_R = 0$;

- the compatibility condition stating the independence of the nonlinear behaviour on the load direction for shear, i.e. $\gamma_{IN}(-\gamma_R) = -\gamma_{IN}(\gamma_R)$

With these conditions the polynomial finally becomes

$$\gamma_{IN} = a\gamma_R^3 + b\gamma_R^5 + - - - \ldots \qquad (19a)$$

During relaxation strict linear behaviour must be assumed due to the correlation of nonlinear creep with the reversible potential barriers. The linear behaviour during relaxation together with the shape of the virgin curve during loading define then the hysteresis properties of the spring G_{3N}, i.e. the hysteresis according to large stresses of long duration t_{LE}. This hysteresis originates in addition to the one caused by the linear irreversible creep (γ_I), treated in section 8.5. In principle, it should be possible with a spring dashpot model extended by eq. (19a) to describe the nonlinear behaviour of any ductile material. The parameters required can be determined by a few creep and relaxation tests at different load levels and temperatures.

The presently available test results only permit the lowest order approximation of eq. (19a), i.e.

$$\gamma_{IN} \propto \gamma_R^3 \ldots \qquad (19b)$$

Equation (19b) is equivalent to

$$\gamma_{IN} \propto \sigma^3$$

The steady-state value $\gamma_{R\infty}$, related to $\sigma = 20$ Mpa, can easily be derived from the test results after relaxation. From the total non-reversible creep (γ_{IT}) after relaxation of Fig. 11 also the steady-state (time-independent) non-linear creep ($\gamma_{IN\infty}$) can be derived

$$\gamma_{IN\infty} = \gamma_{IT} - \dot{\gamma}_\infty t_{LE} \ldots \qquad (19c)$$

It is therefore appropriate to express the non-linear creep finally by

$$\gamma_{IN} = \beta\gamma_{R\infty}(\gamma_R/\gamma_{R\infty})^3 \ldots \qquad (19d)$$

where the constant

$$\beta = \gamma_{IN\infty}/\gamma_{R\infty} \ldots \qquad (19e)$$

was introduced since its temperature dependence is expected to be negligible. From the creep tests follows for β at the different temperatures

$$\beta_{40} = 0.92 \quad \beta_{60} = 0.44 \quad \beta_{80} = 0.66$$

At $T = 40C$ the experimental results are doubtful since the creep values are small compared to the elastic strain. Hence the differences in β are rather to be attributed to scatter than to a dependence on temperature. For quantitative estimates the average of the three values $\beta = 2/3$ will be inserted therefore.

With eq. (19) and the results from section 8.5 for the reversible saturation creep it is now possible to relate the fatigue tests to the actual load shape during operation of the magnet.

8.8 Equivalent Creep Condition

The fatigue tests will represent the cycle encountered during operation of the TF-coils, provided that the total creep displacements coincide, in addition to the maximum load level (σ), cycle number N and temperature (T). It is therefore required to estimate up to which puls length of magnet operation (t_{LO}) the creep encountered will be equivalent to that of the fatigue test. This estimate is simplified by the fact that steady-state conditions can be assumed throughout.

During operation (index O) of the TF-coils the average spring elongation of the simplified dashpot model (section 8.6) will be zero. Consequently there is nether a contribution by reversible nor by nonlinear creep to be expected. Thus the only contribution results from linear irreversible creep according to eq. (1)

$$\gamma_{IO} = \dot{\gamma}_{\infty} t_{LO} N_O$$

The creep originating during a fatigue test (index F) is composed of three components

- the reversible saturation creep which is according to section 8.6

$$\gamma_{RSF} = 1/2\gamma_{R\infty}$$

- the nonlinear creep correction which follows from eq. (19) with $\gamma_R = \gamma_{RSF}$ to be

$$\gamma_{IN} = \gamma_{IN\infty}/8 = \beta\gamma_{R\infty}/8 = \beta\gamma_{RSF}/4$$

- the linear irreversible creep of the preceding creep test of duration $t = t_{CT}$ (a nonlinear contribution can be neglected) together with the contribution during cycling according to eq. (1)

$$\gamma_{IF} = \dot{\gamma}_\infty(t_{CT} + t_{LF} \cdot N_F)$$

The condition of creep equivalence yields then for the maximum equivalent pulse duration

$$t_{LO} \leq \frac{N_F}{N_0} t_{LF} + \left(\frac{1}{2}\frac{\gamma_{R\infty}}{\dot{\gamma}_\infty}(1 + \beta/4) + t_{CT}\right)/N_0 \ldots \qquad (20)$$

For $N_F = N_O = 20000$, $t_{CT} = 10000$ s and $t_{LF} = 2$ s it follows for $T = 60C$ from eq. (20)

$$t_{LO} \lesssim 6.3\,\text{sec.}$$

The contributions to the equivalent pulse duration of the 10.000 s creep test and the nonlinear creep are negligible. Each of them is just about 8%.

The main contribution to the equivalent pulse duration results from the reversible saturation creep encountered during cycling. Therefore the 0.25 Hz fatigue test represents also with respect to creep the circumstances encountered during operation of the TF-coils.

9. SUMMARY

The tests performed have consistently shown that a flexibilizer content of 10 to 15 PoW is required for the combination of ARALDIT-F with hardener HT 907. This standard resin system can then be subjected to a shear stress of 25 Mpa for N = 20,000 cycles at $T \lesssim 60$ C.

The application of torque tube specimens has opened the possibility for precise strain measurement. By quantitative assessment of the creep strain it was shown that the fatigue tests are also relevant for the total insulation creep originating during the envisaged operation of the TF coils.

The creep tests at σ=20 Mpa have shown a considerable nonlinear component. This component depends at least on the third power of the stress and is therefore negligible below $\sigma = 10$ Mpa. For the same reason the impact of nonlinear creep on the fatigue tests in only marginal.

Failure of the insulation system develops during cycling only gradually. The first indication is a noticeable hysteresis width followed then by a drop of the shear modulus. During operation of the TF-coils this behaviour should permit to detect overloading prior to a major damage.

Acknowledgement

The authors like to thank H.R. Aus der Au from CIBA-GEIGY (Basel) for his valuable support during the definition period of the insulation system and the related coil curing procedure.

REFERENCES

[1] A. Puck, H. Schürmann, Kunststoffe 72, 1982, Heft 9, pp 554–561.
[2] I. Engesser, A. Puck, Kunststoffe 70, 1980, Heft 7, pp 423–429.
[3] H. Lee, K. Neville, Handbook of Epoxy Resins, McGraw Hill, New York 1967.
[4] B. Streibl, E. Springmann, O. Jandl, MT-9 Conference, Grenoble, 1983, pp C1-163.
[5] O. Hahn, G. Kötting, Schweißen und Schneiden 36, 1984, Heft 6.
[6] W. Holzmüller, K. Kaltenburger, Physik der Kunststoffe, Berlin, 1961.
[7] I. Cowie, Chemie und Physik der Polymeren, New York 1976.
[8] W. Holzmüller. E. Jenckel, Zeitschr. Physik Chem.(A) 186, p.359, 1940.
[9] W. Holzmüller, Physik.Zeitschr.XLII, p.273, 1941.

Figure Captions

Fig. 1: Results of cyclic tension tests with pure resin specimens.

Fig. 2: Density-temperature diagram of a typical epoxy resin from [3].

Fig. 3: Insulation system of a TF coil.

Fig. 4: Test device for tube specimen.

Fig. 5: Device for aligning and impregnating the long tube specimen.

Fig. 6: Holders for short tube specimen.

Fig. 7: Shear stress versus shear angle - rupture test.

Fig. 8: Shear displacement - cyclic test with tube specimen.

Fig. 9: Development of the hysteresis during a cyclic test.

Fig. 10: Typical displacement behaviour during a creep test.

Fig. 11: Temperature dependence of creep (F5 tube specimen).

Fig. 12: Dashpot/spring creep model.

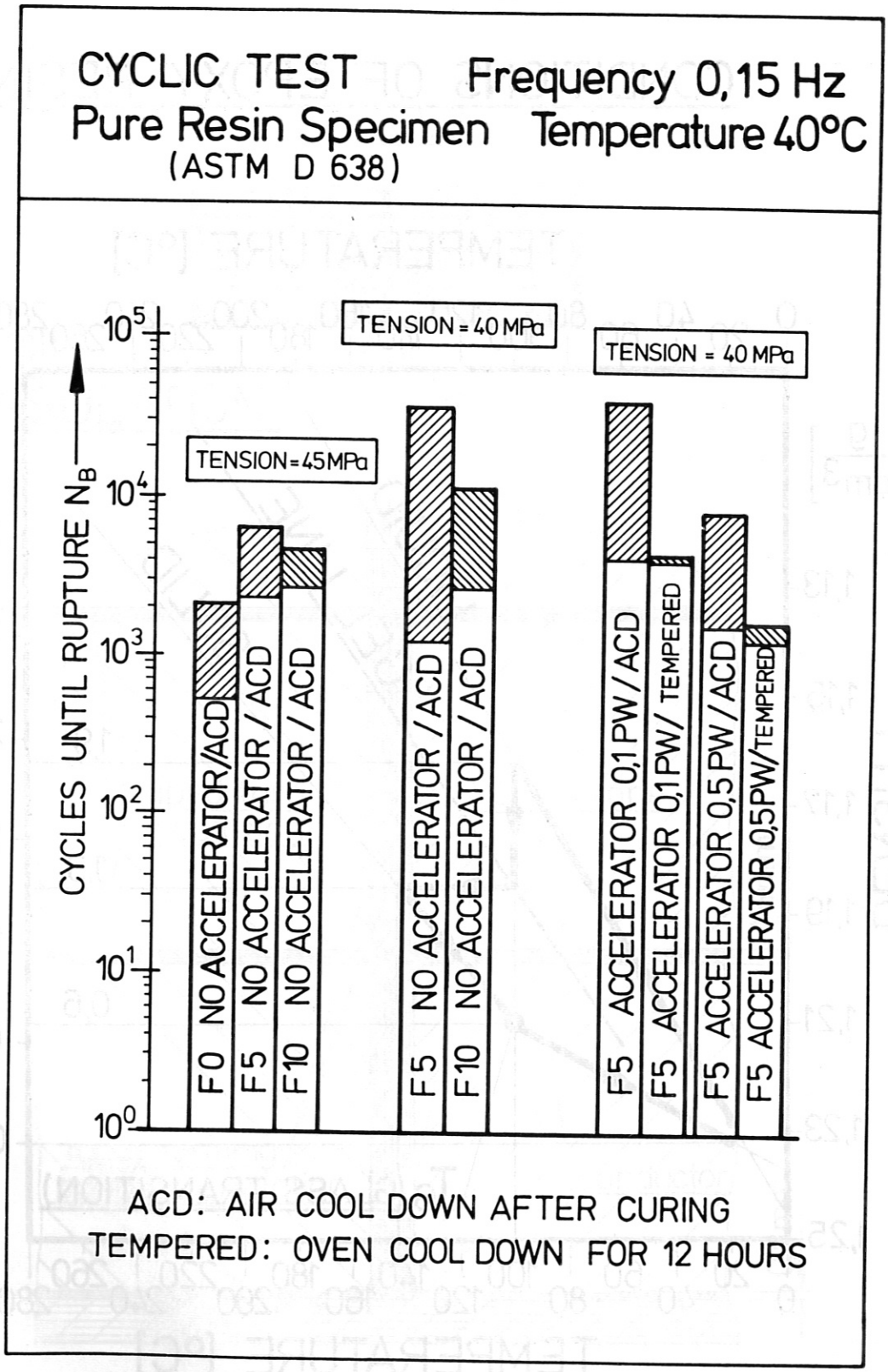

Fig. 1: Results of cyclic tension tests with pure resin specimens.

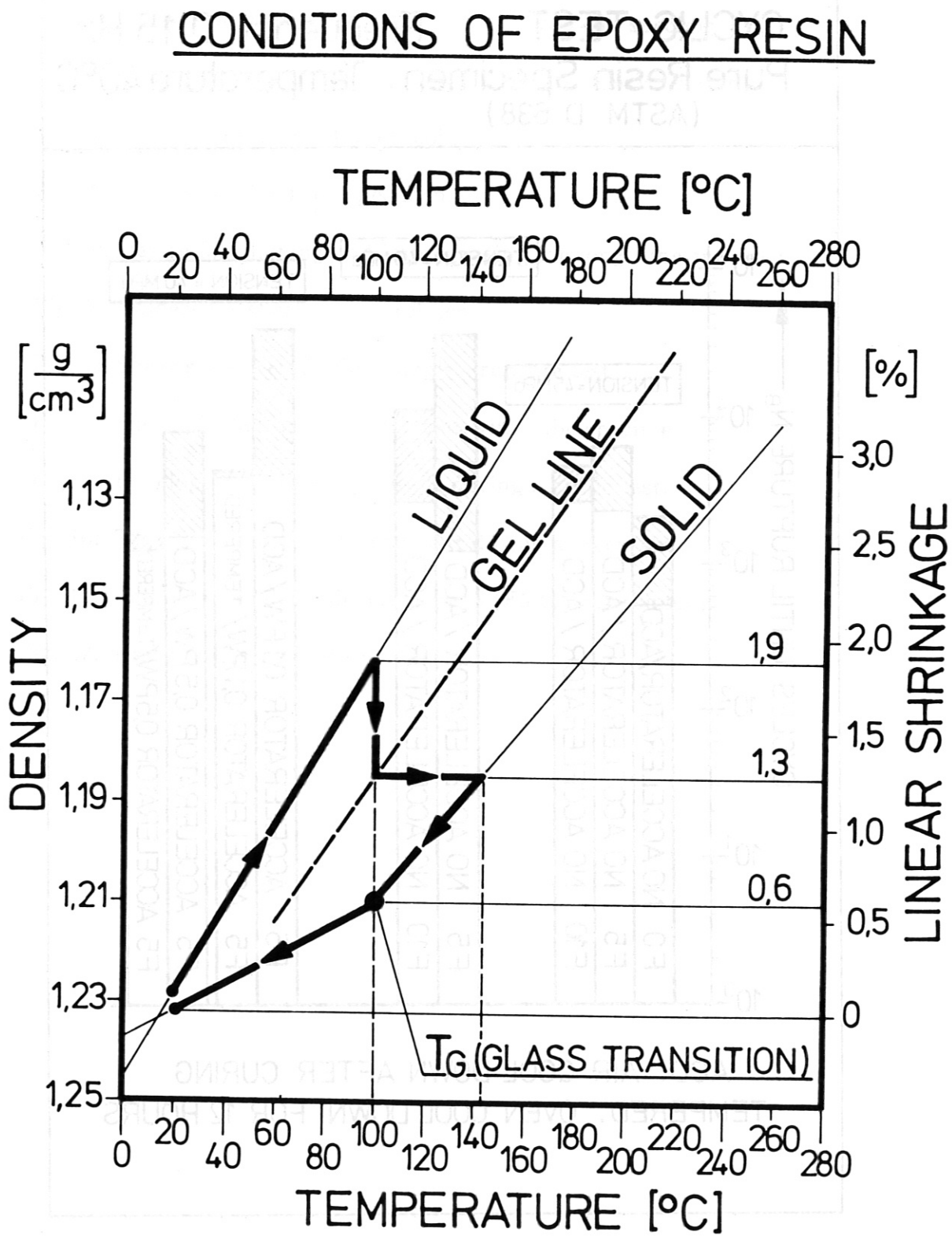

Fig. 2: Density-temperature diagram of a typical epoxy resin from [3].

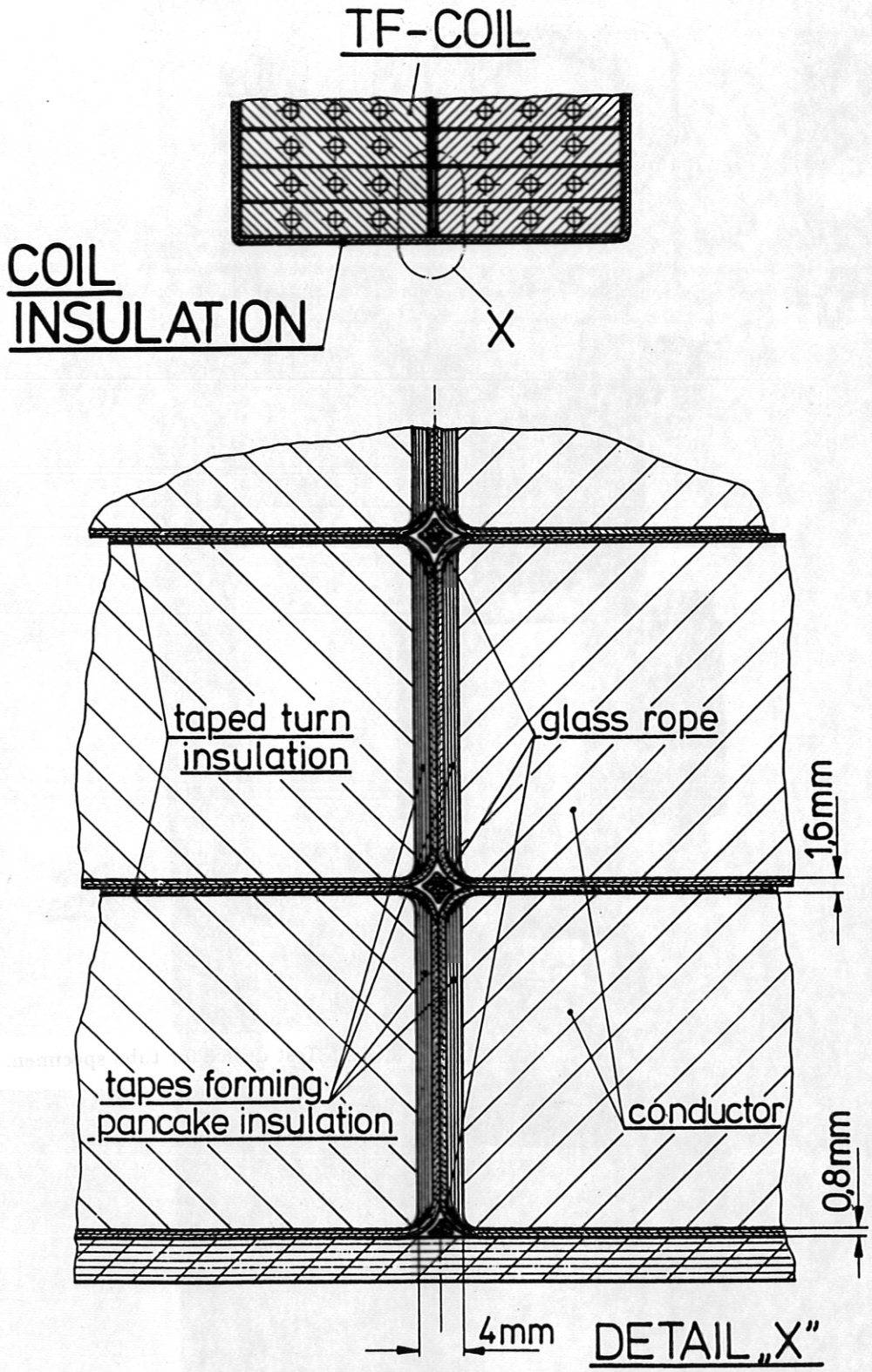

Fig. 3: Insulation system of a TF coil.

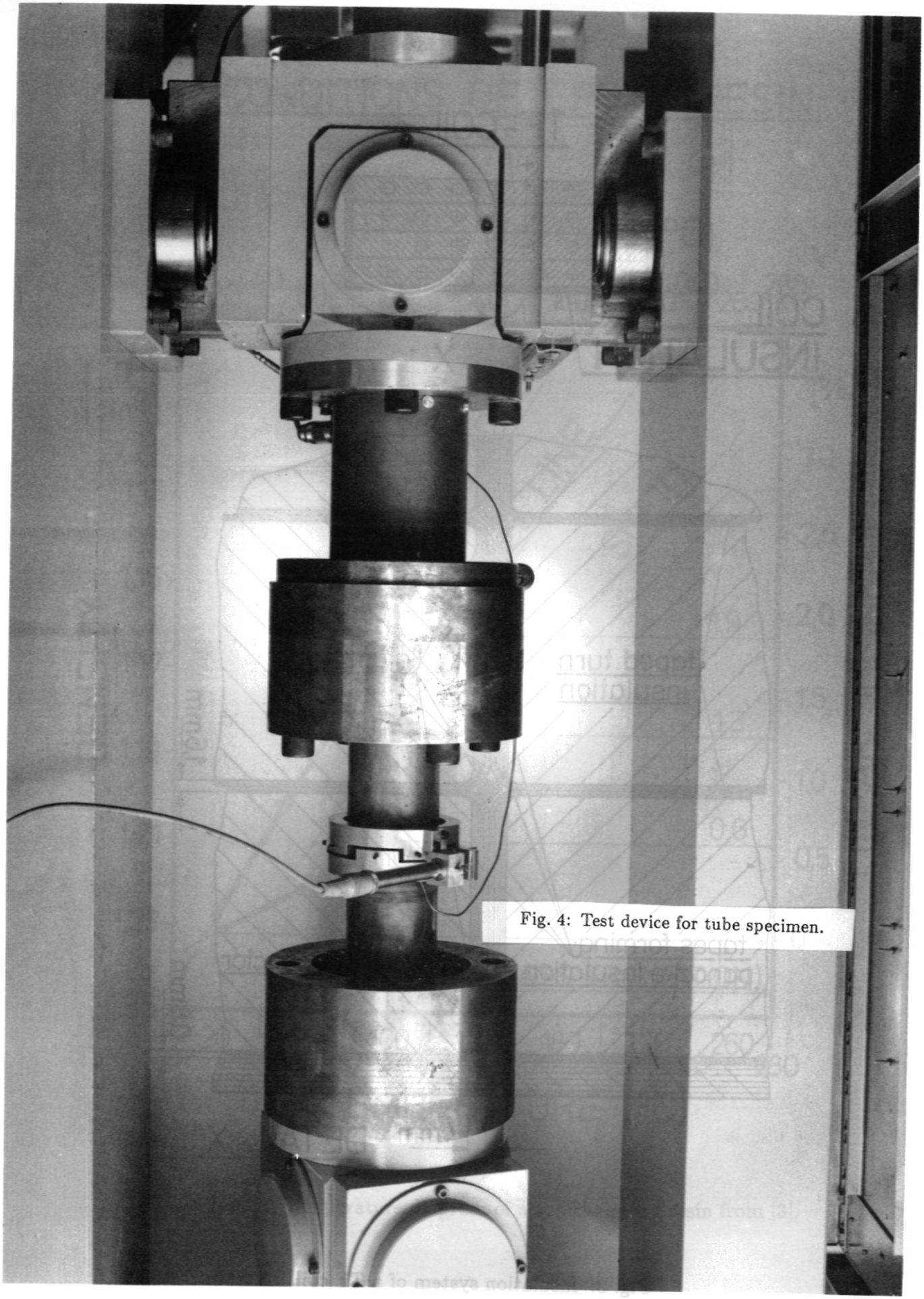

Fig. 4: Test device for tube specimen.

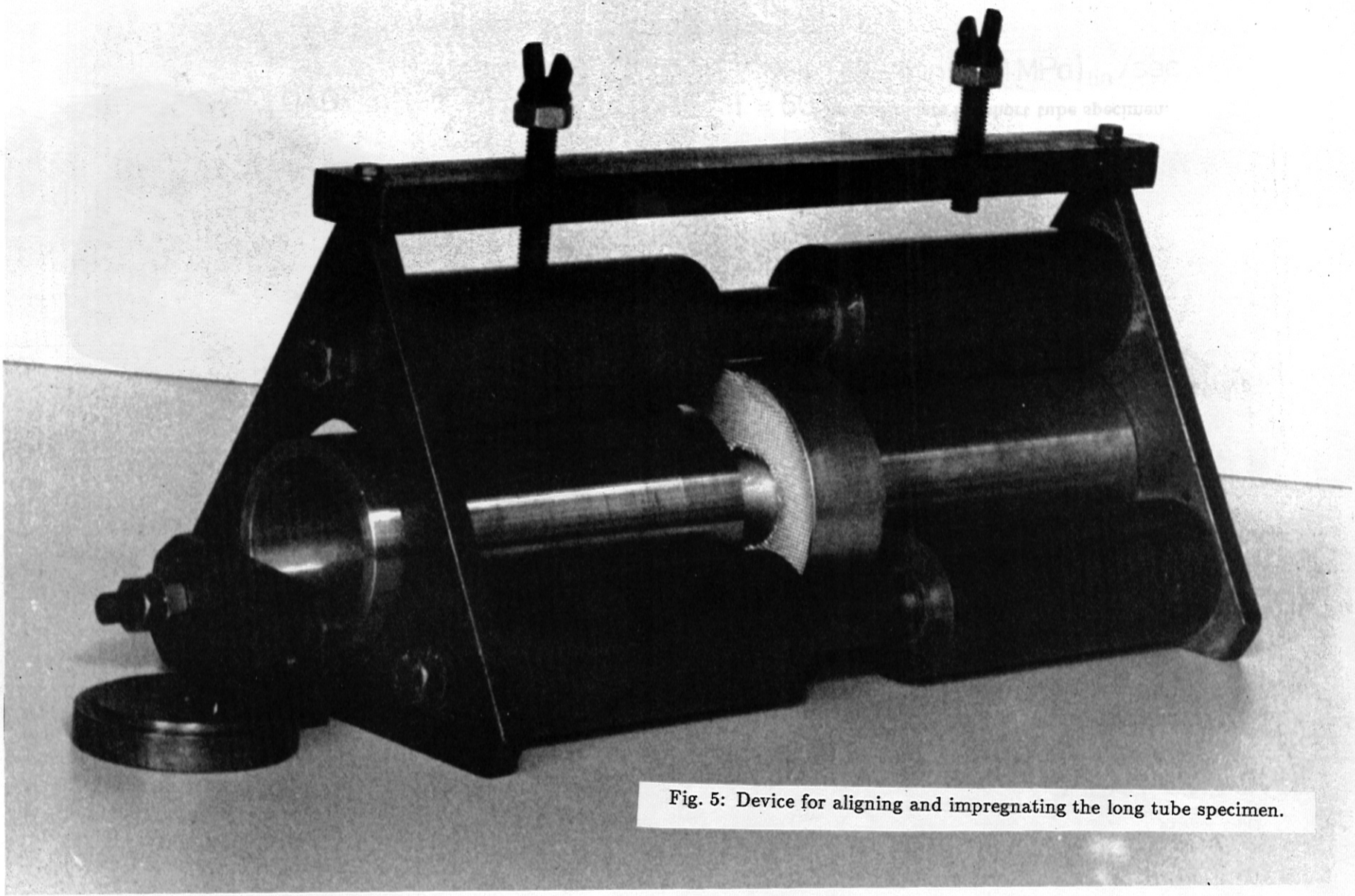

Fig. 5: Device for aligning and impregnating the long tube specimen.

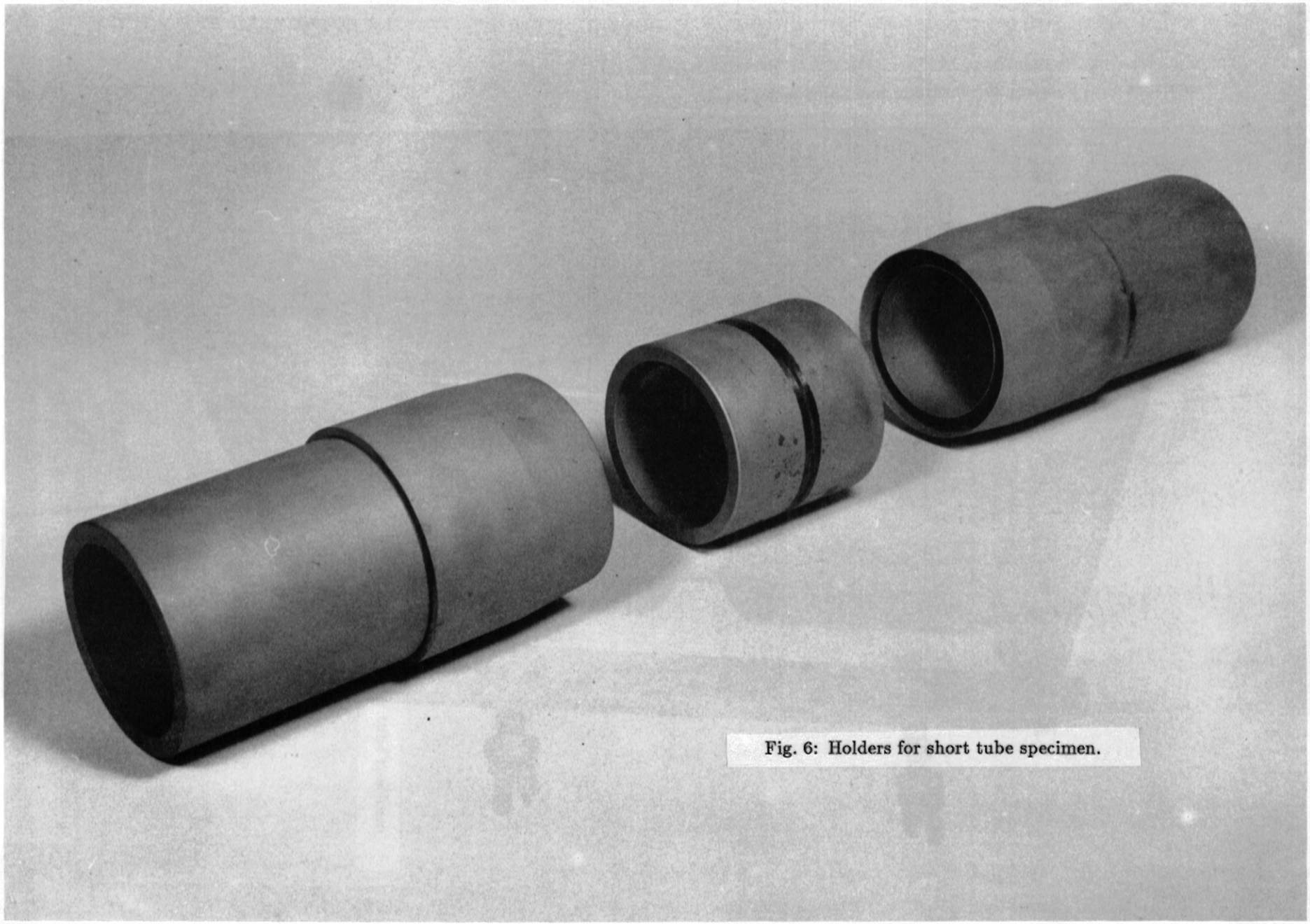

Fig. 6: Holders for short tube specimen.

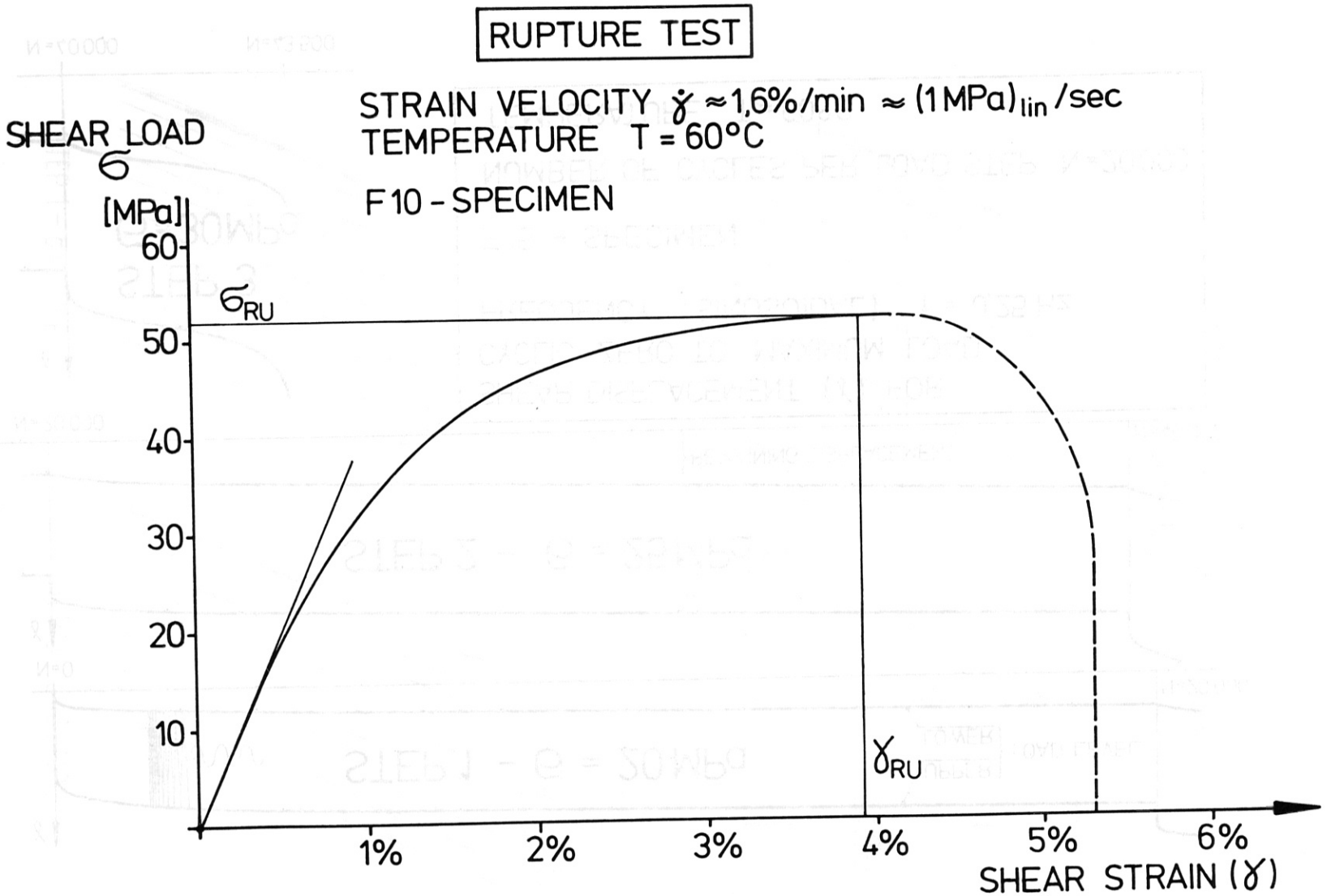

Fig. 7: Shear stress versus shear angle - rupture test.

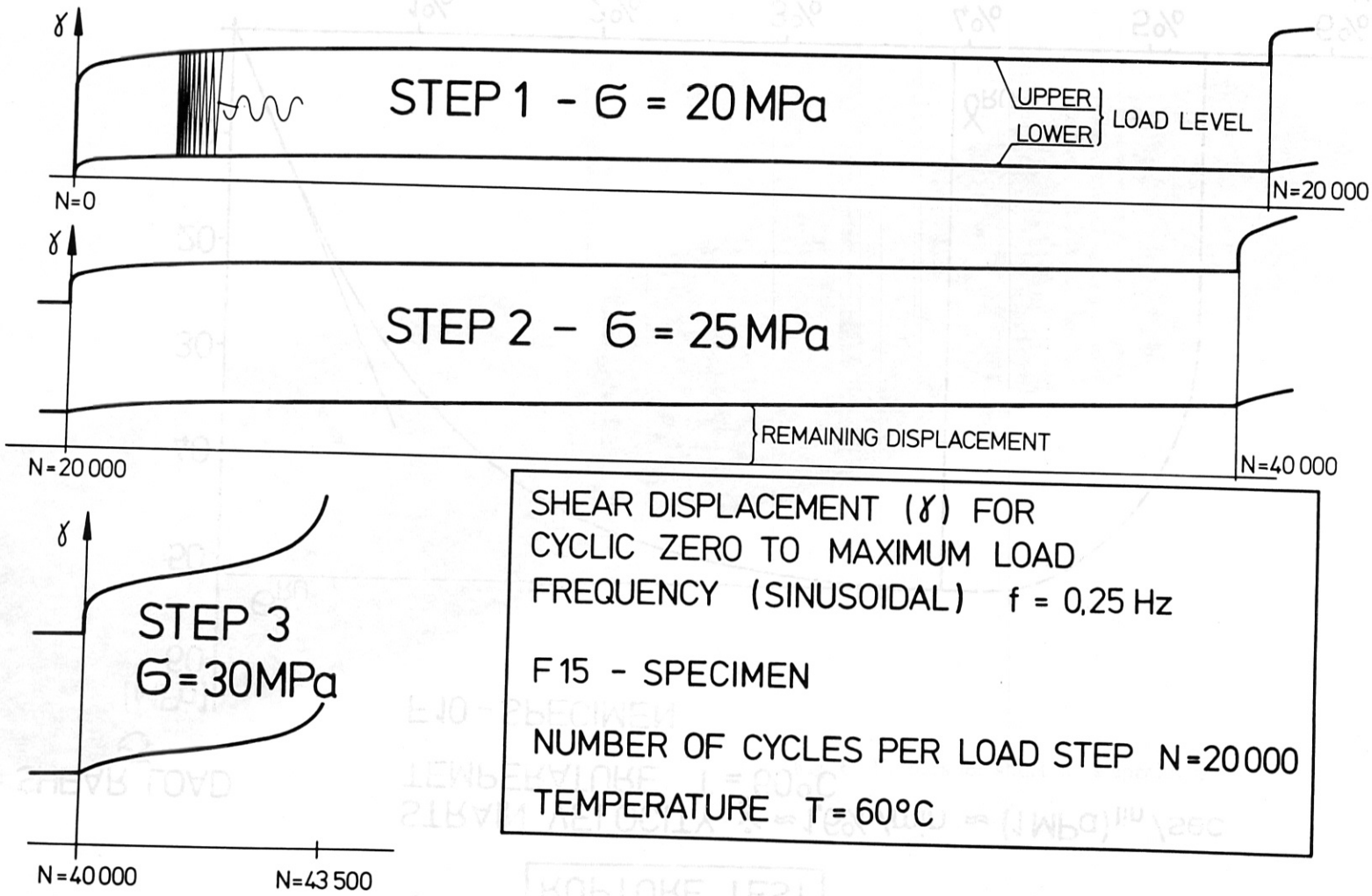

Fig. 8: Shear displacement - cyclic test with tube specimen.

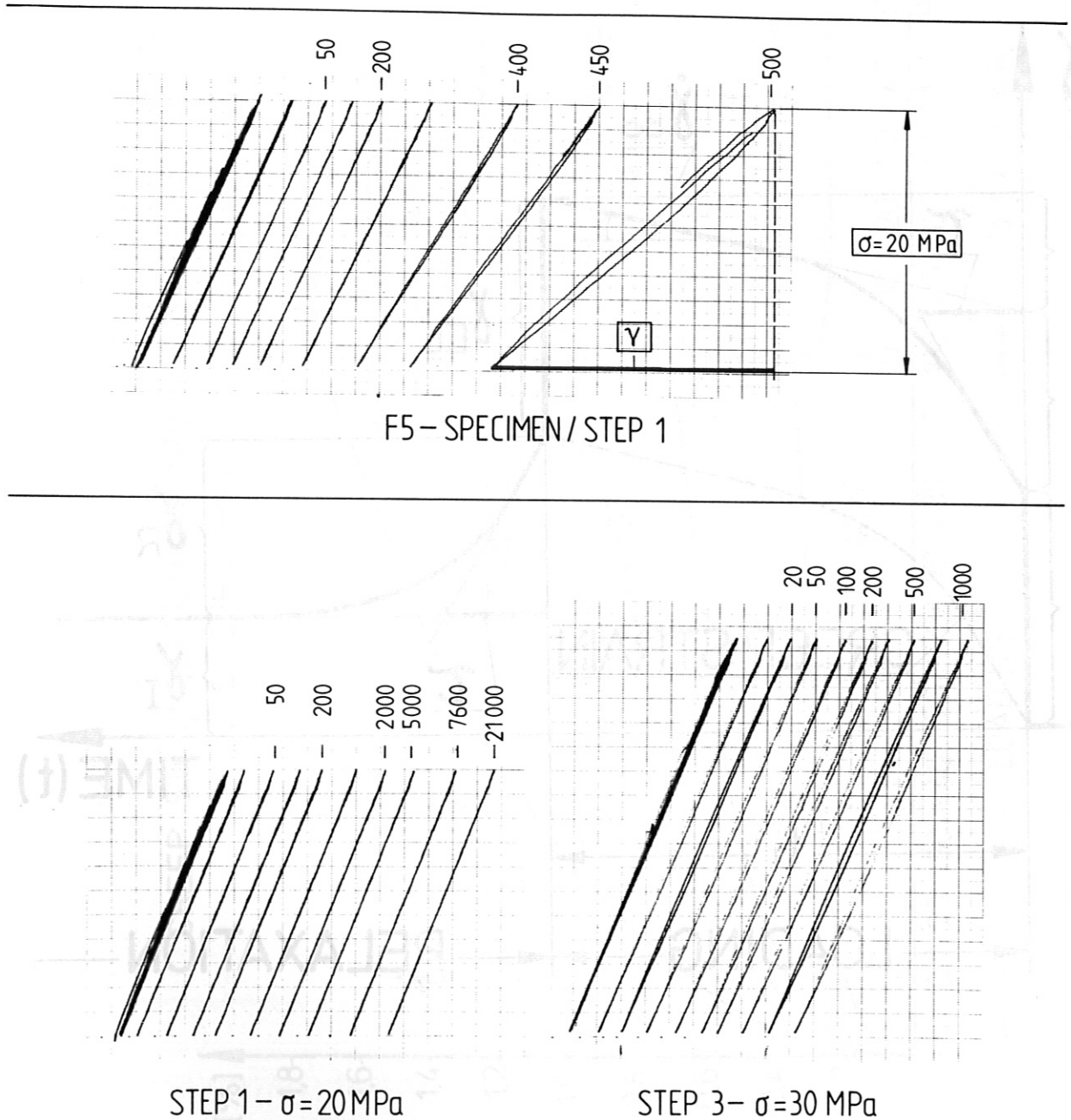

Fig. 9: Development of the hysteresis during a cyclic test.

$$\gamma_I = \dot{\gamma}_\infty \cdot t_L$$

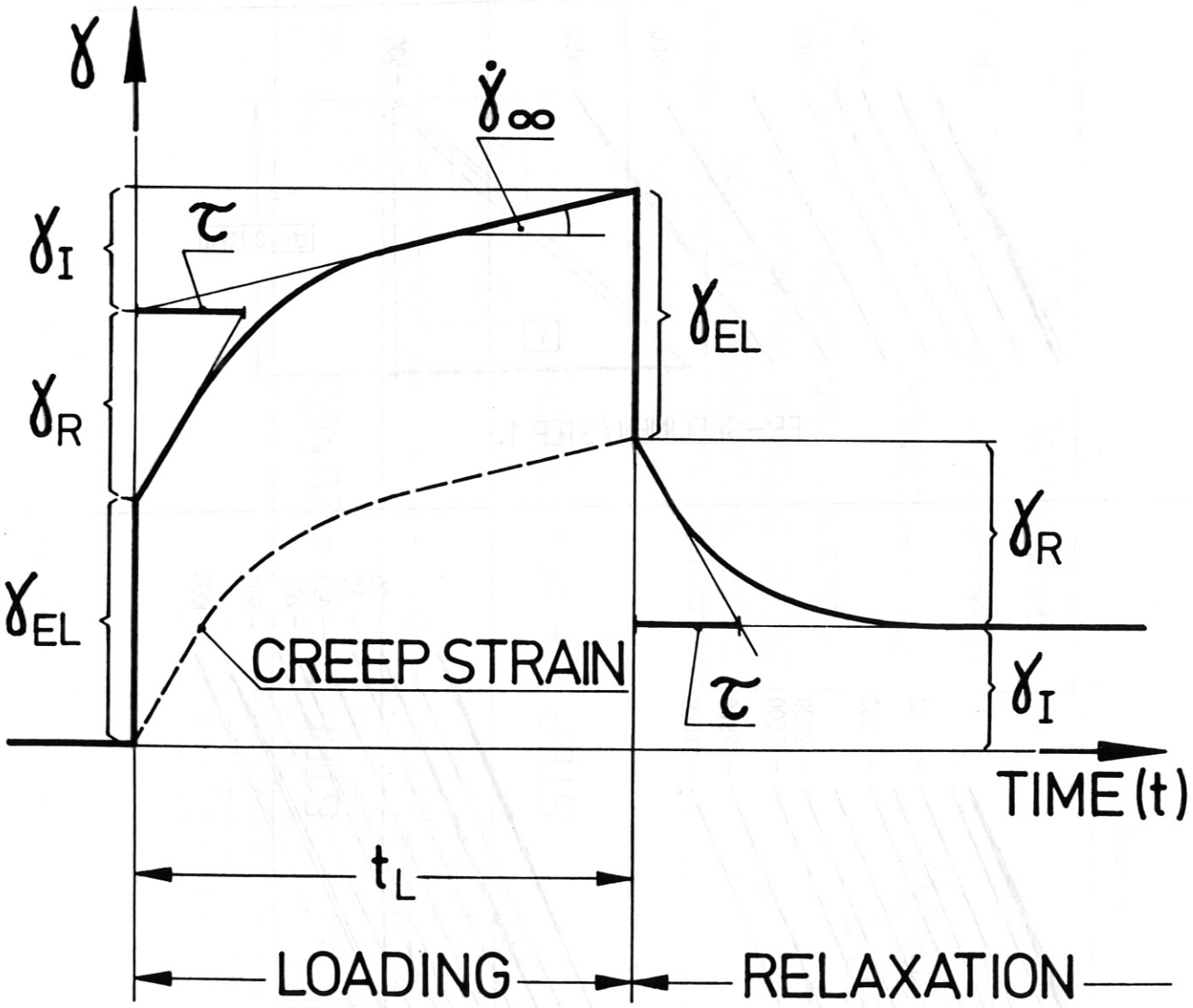

Fig. 10: Typical displacement behaviour during a creep test.

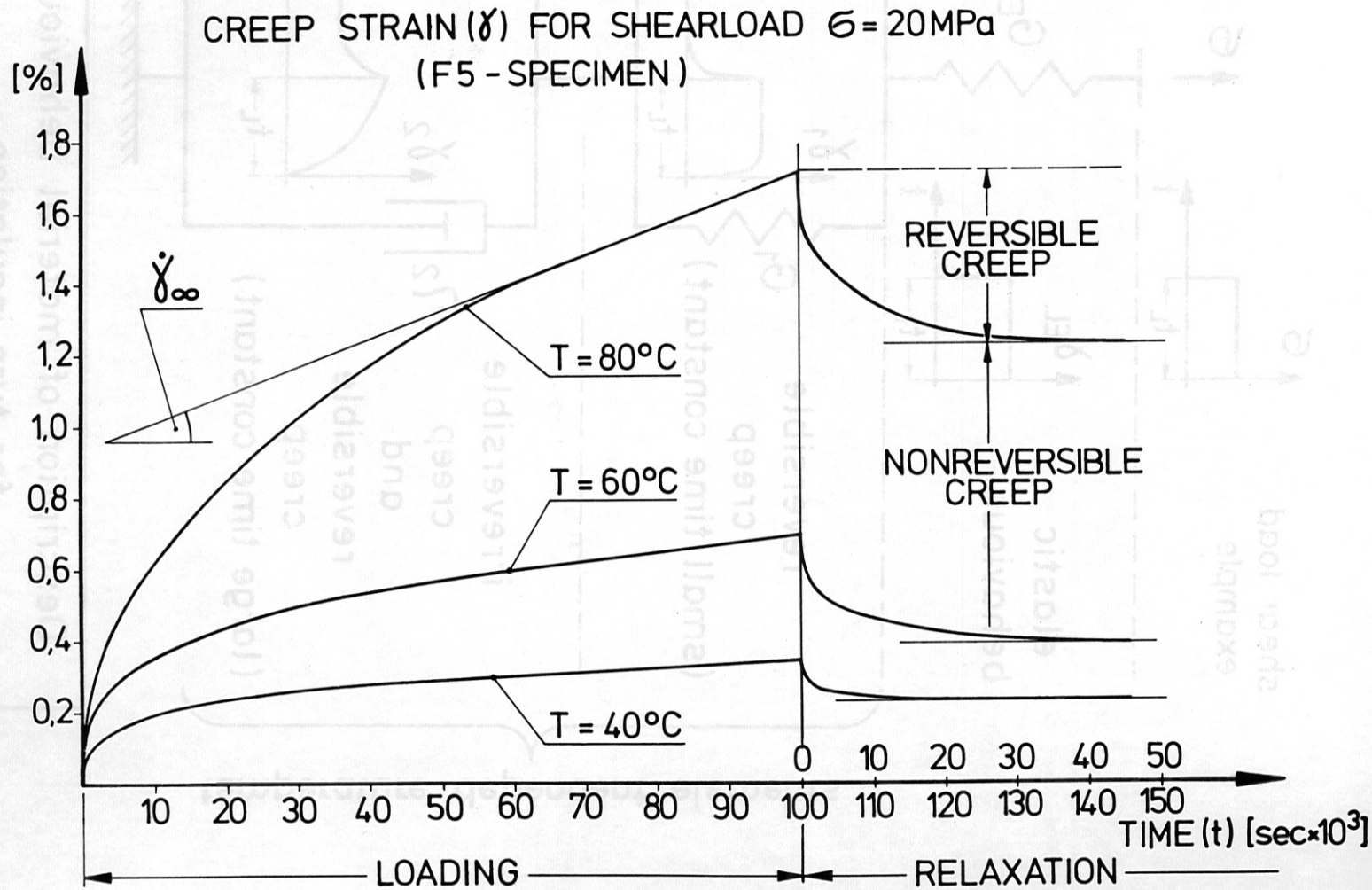

Fig. 11: Temperature dependence of creep (F5 tube specimen).

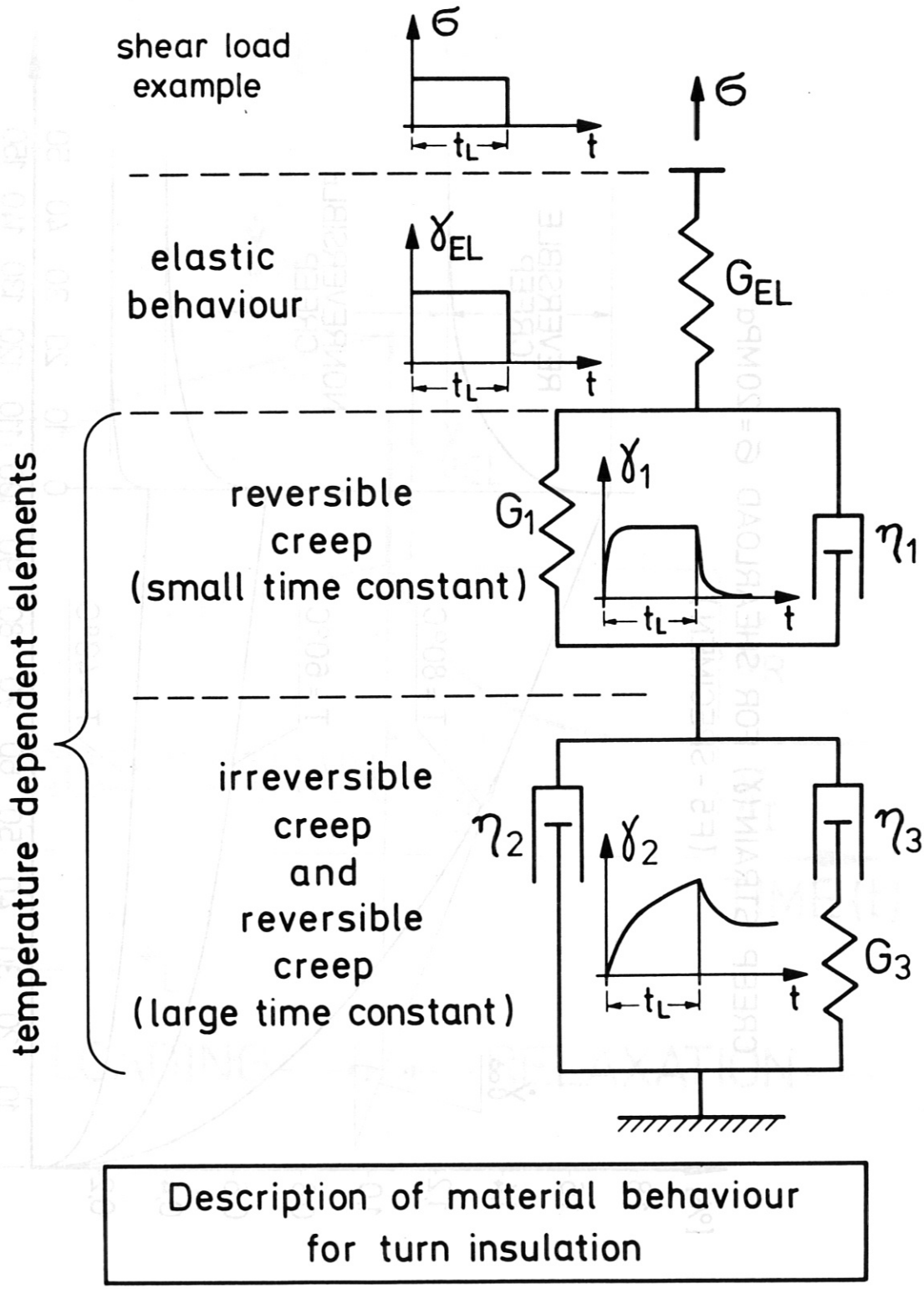

Fig. 12: Dashpot/spring creep model.